Hybrid WENO schemes for polydisperse sedimentation models

G. Chiavassa

Laboratoire de Mècanique, Modélisation et Procédés Propres, UMR 6181 CNRS-ECM, Technopôle de Chateau-Gombert, 38 rue Joliot-Curie, 13451 Marseille, France

M.C. Martí

CI^{2}MA and Departamento de Ingeniería Matemática, Facultad de Ciencias Físicas y Matemáticas, Universidad de Concepción, Casilla 160-C, Concepción, Chile

P. Mulet

Departament de Matemàtica Aplicada, Universitat de València, Av. Vicent Andrés Estellés, s/n, 46100, Burjassot, Spain

Abstract

Polydisperse sedimentation models can be described by a strongly coupled system of conservation laws for the concentration of each species of solids. Typical solutions for the sedimentation model considered for batch settling in a column include stationary kinematic shocks separating layers of sediment of different composition. This phenomenon, known as segregation of species, is a specially demanding task for numerical simulation due to the need of accurate numerical simulations.

Very high-order accurate solutions can be constructed by incorporating characteristic information, available due to the hyperbolicity analysis made in [R. Donat and P. Mulet, *A secular equation for the Jacobian matrix of certain multispecies kinematic flow models*, Numer. Methods Partial Differential Equations, 26 (2010), pp. 159–175.] But characteristic-based schemes, see [R. Bürger, R. Donat, P. Mulet, and C. A. Vega, *On the implementation of WENO schemes for a class of polydisperse sedimentation models*, J. Comput. Phys., 230 (2011), pp. 2322–2344], are very expensive in terms of computational time, since characteristic information is not readily available, and they are not really necessary in constant areas, where a less complex method can obtain similar results. With this idea in mind, in this paper we develop a hybrid finite difference WENO scheme that only uses the characteristic information of the Jacobian matrix of the system in those regions where singularities exist or are starting to develop, while it uses a component-wise approximation of the scheme in smooth regions.

Email addresses: guillaume.chiavassa@centrale-marseille.fr (G. Chiavassa), mmarti@ci2ma.udec.cl (M.C. Martí), mulet@uv.es (P. Mulet)

We perform some experiments showing the computational gains that can be achieved by this strategy.

Keywords: Finite difference WENO schemes, component-wise schemes, polydisperse sedimentation

2000 AMS Subject Classifications: 35L65; 65M06; 76T20

---

1. Introduction

High Resolution Shock Capturing (HRSC) schemes are one of the most important tools used nowadays to compute accurate numerical approximations to the solution of many hyperbolic systems of conservation laws. They are usually developed combining an upwind framework, i.e, taking into account the direction of propagation of the information, and a high order interpolatory technique to prevent the development of spurious numerical oscillations.

Most of these HRSC schemes require a specific knowledge of the spectral decomposition of the Jacobian matrix of the system, since the eigenvalues and eigenvectors are used to compute the numerical approximations by local projections to characteristic fields. The numerical solutions that we obtain are often excellent in terms of resolution power. However, in many cases, as in sedimentation models for polydisperse suspensions, the spectral information is quite difficult to obtain, due to the lack of closed formulas for the eigenstructure of the flux Jacobian. Therefore, the computational effort needed to apply these complex techniques may be fairly considerable.

When solving hyperbolic systems of conservation laws, non-smooth structures might develop spontaneously and evolve in time. Resolving adequately those regions of strong variation requires the use of very fine grids. But, taking into account that we are working with uniform meshes, the solution will be over resolved in regions where it is smooth.

It is well known that the costly numerical computations involved in these schemes are only necessary at existing singularities or when these are about to form. Consequently, we can reduce the computational cost of the scheme, while maintaining its high-order properties, by using expensive resources only at the neighborhood of a singularity.

Many adaptive techniques, which aim to concentrate the computational effort near singularities or sharp transition regions, have been developed in the literature [9, 15, 19]. The most remarkable examples are the Multiresolution strategy, based on the multilevel strategies first introduced by Harten in [12], and the Adaptive Mesh Refinement (AMR) techniques [1, 2].

In this work, we propose a hybrid scheme that substitutes the costly characteristic based computation of the numerical fluxes by a component-wise approach of the scheme when the solution is smooth enough. We use polydisperse sedimentation models to test the efficiency of the hybrid scheme mainly for two reasons: First, because of the high computational effort needed to compute the spectral information which have to be computed in the SPECINT scheme. If

the spectral information is easily available this hybrid scheme, as well as multiresolution schemes, can not improve the results obtained in terms of efficiency. Secondly because it is near sharp transitions where we need to improve the approximate results without increasing the computational cost and we know that the typical solutions for the sedimentation model considered for batch settling in a column include stationary kinematic shocks separating layers of sediment of different composition which is a special demanding task for numerical simulation due to the need of accurate numerical simulations.

The paper is organized as follows: First of all, in section 2, we recall the basic facts of the Masliyah-Lockett-Bassoon (MLB) polydisperse sedimentation model [16, 17], its hyperbolicity and bounds on characteristic speeds. In section 3, we briefly describe the main ingredients of finite difference WENO schemes. In section 4 we explain the basic strategy used in our cost-effective alternative to characteristic-based schemes and in section 5 we perform some numerical experiments and analyze the quality of the numerical approximations obtained with the hybrid scheme and its efficiency. Finally, we draw some conclusions in section 6.

2. Polydisperse sedimentation models

Polydisperse suspensions are mixtures composed of small solid particles belonging to M different species, that vary in size or density, and which are dispersed in a viscous fluid. We denote the diameter of the i-th species as D_i and we assume the species to be ordered so that $D_1 > D_2 > \cdots > D_M$. In this work, we will only consider particles of the same density.

If we denote ϕ_i as the volume fraction of particle species i and v_i for the phase velocity of species i, then the continuity equations of the M species are

$$\partial_t \phi_i + \partial_x(\phi_i v_i) = 0, \quad i = 1, \ldots, M,$$

where t is time and x is depth.

The velocities $v_1, \ldots, v_M$ are assumed to be given functions of the vector of local concentrations $\Phi := \Phi(x,t) := (\phi_1(x,t), \ldots, \phi_M(x,t))^{\mathrm{T}}$ (kinematic assumption). This yields nonlinear, strongly coupled systems of conservation laws of the type

$$\Phi_t + f(\Phi)_x = 0, \tag{1}$$

where the components of the flux function $f(\Phi) = (f_1(\Phi), \ldots, f_M(\Phi))^T$ are given by $f_i(\Phi) := \phi_i v_i(\Phi),\ i = 1, \ldots, M$.

We seek solutions $\Phi = \Phi(x,t)$ such that $\phi_i \geq 0,\ \forall i = 1, \ldots, M$, and $\phi := \sum_{i=1}^{M} \phi_i \leq \phi_{\max}$, where the parameter $\phi_{\max} \in (0,1]$ stands for a given maximum solids concentration.

The velocity model for polydisperse sedimentation considered in this work is the Masliyah-Lockett-Bassoon (MLB) model [16, 17], which is one of the most commonly used velocity models for polydisperse sedimentation. It arises from

the continuity and linear momentum balance equations for the solid species and the fluid through suitable constitutive assumptions and simplifications (cf. [3]). For particles that have the same density, the velocities $v_1(\Phi), \dots, v_M(\Phi)$ are given by

$$v_i(\Phi) = \nu(1-\phi)V(\phi)\big(d_i^2 - (\phi_1 d_1^2 + \cdots + \phi_M d_M^2)\big), \quad \nu = \frac{(\varrho_{\mathrm{s}} - \varrho_{\mathrm{f}})gD_1^2}{18\mu_{\mathrm{f}}},$$

where ϱ_{s} and ϱ_{f} are the solid and fluid densities respectively, g is the acceleration of gravity, d_i are the normalized particle sizes $d_i = D_i/D_1$ for $i = 1, \dots, M$, μ_{f} is the fluid viscosity and V is an empirical hindered settling function assumed to satisfy

$$V(0) = 1, \quad V(\phi_{\max}) = 0, \quad V'(\phi) \le 0 \quad \text{for } \phi \in [0, \phi_{\max}].$$

A standard choice for $V(\phi)$ is given by Richardson-Zaki's hindered settling function [20]:

$$V(\phi) = \begin{cases} (1-\phi)^{n_{RZ}-2}, & 0 \le \phi \le \phi_{max}; \\ 0, & \text{otherwise.} \end{cases}$$

with $n_{\mathrm{RZ}} > 2$, $\phi_{max} < 1$.

For the typical application of batch settling of a suspension in a column of height $L > 0$, (1) is defined for $(x,t) \in (0,L) \times (0,T)$ and zero-flux boundary conditions are prescribed:

$$f|_{x=0} = f|_{x=L} = 0.$$

As it can be seen in [3, 10], the MLB model is strictly hyperbolic whenever $\phi_i > 0$ for all $i = 1, \dots, M$, and $\phi < \phi_{\max}$. The eigenvalues $\lambda_i = \lambda_i(\Phi)$ of the Jacobian matrix $f'(\Phi)$ satisfy the interlacing property

$$v_{M+1}(\Phi) < \lambda_M(\Phi) < v_M(\Phi) < \lambda_{M-1}(\Phi) < v_{M-1}(\Phi) < \cdots < \lambda_1(\Phi) < v_1(\Phi) \tag{2}$$

where the lower bound is given by

$$v_{M+1}(\Phi) = \nu\Big(d_M^2 V(\Phi) + \big((1-\phi)V'(\phi) - 2V(\phi)\big)(d_1^2\phi_1 + \cdots + d_M^2\phi_M)\Big).$$

3. Finite difference WENO schemes

In order to simplify the notation, let us restrict ourselves to one-dimensional scalar conservation laws with properly prescribed initial and boundary conditions on some interval, which can be written as:

$$\Phi_t + f(\Phi)_x = 0. \tag{3}$$

Finite differences WENO schemes (see [23]) can be naturally extended to multiple dimensions by design and to systems via local characteristic decompositions.

First of all, we consider a uniform grid on $[0, L]$ defined by the points $x_i = \left(i - \frac{1}{2}\right)\Delta x, i = 1, \ldots, N$, which are the centers of the cells whose boundaries are given by $x_{i+\frac{1}{2}} = x_i + \frac{\Delta x}{2}$, where $\Delta x = L/N$ is the uniform grid spacing, so that, the boundaries of the interval $[0, L]$ are $0 = x_{\frac{1}{2}}$ and $L = x_{N+\frac{1}{2}}$.

In order to obtain high order finite difference conservative schemes to solve (3), we use Shu and Osher's technique [23], for which the conservative property of the spatial discretization is obtained by implicitly defining, for fixed $t, \Delta x$, the function φ as:

$$f(\Phi(x,t)) = \frac{1}{\Delta x}\int_{x-\frac{\Delta x}{2}}^{x+\frac{\Delta x}{2}} \varphi(\xi)d\xi,$$

so that the spatial derivative in (3) is exactly obtained by a conservative finite difference formula that involves values of φ at the cell boundaries,

$$f(\Phi(x,t))_x = \frac{1}{\Delta x}\left(\varphi\left(x + \frac{\Delta x}{2}\right) - \varphi\left(x - \frac{\Delta x}{2}\right)\right).$$

We can compute highly accurate approximations to $\varphi\left(x \pm \frac{\Delta x}{2}\right)$, denoted by $\widehat{\varphi}$, using known grid values of $f(\Phi)$ (which are cell-averages of φ) and a reconstruction method $\mathcal{R}$ (a function whose cell-averages coincide with the given ones) as $\varphi(x_{i+\frac{1}{2}}) = \widehat{\varphi}(x_{i+\frac{1}{2}}) + d(x_{i+\frac{1}{2}})\Delta x^r + \mathcal{O}(\Delta x^{r+1})$, with d a Lipschitz function, where

$$\widehat{\varphi}(x) = \mathcal{R}(f_{i-p}, \ldots, f_{i+q}; x), \quad f_l = f(\Phi(x_l, t)).$$

We can thus discretize the spatial derivative in Equation (3) as:

$$(f(\Phi))_x(x_i) = \frac{\hat{f}_{i+\frac{1}{2}} - \hat{f}_{i-\frac{1}{2}}}{\Delta x} + \mathcal{O}(\Delta x^r), \quad \hat{f}_{i+\frac{1}{2}} = \widehat{\varphi}(x_{i+\frac{1}{2}}).$$

The spatially-discretized problem

$$\Phi_i'(t) = \mathcal{D}(\Phi(t))_i, \quad \Phi_k = [\phi_{1,k}, \ldots, \phi_{M,k}]^T, \quad \mathcal{D}(\Phi)_i = \frac{\hat{f}_{i+\frac{1}{2}}(\Phi) - \hat{f}_{i-\frac{1}{2}}(\Phi)}{\Delta x},$$

for approximations $\Phi_i(t) \approx \Phi(x_i, t)$, can be solved using an appropriate ODE solver. In this paper we use the third order TVD Runge-Kutta scheme proposed in [22, 23]:

$$\begin{cases} \Phi^{(1)} = \Phi^n - \Delta t\mathcal{D}(\Phi^n), \\ \Phi^{(2)} = \frac{3}{4}\Phi^n + \frac{1}{4}\Phi^{(1)} - \frac{1}{4}\Delta t\mathcal{D}(\Phi^{(1)}), , \\ \Phi^{n+1} = \frac{1}{3}\Phi^n + \frac{2}{3}\Phi^{(2)} - \frac{2}{3}\Delta t\mathcal{D}(\Phi^{(2)}), \end{cases} \tag{4}$$

where $\Phi_i^n \approx \Phi_i(t_n)$.

To extend these schemes to systems of conservation laws, if we know the full spectral decomposition of the Jacobian matrix $f'(\Phi)$ then we can compute the

numerical flux $\widehat{f}_{i+\frac{1}{2}} := \widehat{\varphi}(x_{i+\frac{1}{2}})$ using an upwind characteristic-wise scheme as:

$$\begin{aligned}\widehat{f}_{i+\frac{1}{2}} = &\sum_{k=1}^{M} r^k \left(\mathcal{R}^+ \left(l^k \cdot f^{+,k}_{i-2}, \ldots, l^k \cdot f^{+,k}_{i+2}; x_{i+\frac{1}{2}}\right)\right) \\ &+ \sum_{k=1}^{M} r^k \left(\mathcal{R}^- \left(l^k \cdot f^{-,k}_{i-1}, \ldots, l^k \cdot f^{-,k}_{i+3}; x_{i+\frac{1}{2}}\right)\right),\end{aligned} \tag{5}$$

where $r^k = r^k(\Phi_{i+\frac{1}{2}})$, $l^k = l^k(\Phi_{i+\frac{1}{2}})$, are the right and left normalized eigenvectors corresponding to the eigenvalue $\lambda_k(f'(\Phi_{i+\frac{1}{2}}))$ of the flux Jacobian $f'(\Phi_{i+\frac{1}{2}})$, respectively, computed at $\Phi_{i+\frac{1}{2}} = \frac{1}{2}\big(\Phi_i + \Phi_{i+1}\big)$, for $k = 1, \ldots, M$. The functions $f^{\pm,k}$ define a flux-splitting, i.e., they verify $f^{+,k} + f^{-,k} = f$, and are upwind fluxes, i.e., $\pm\lambda^k \left((f^{\pm,k}(\Phi))'\right) \geq 0$. In (5) we denote $f_i^{\pm,k} := f^{\pm,k}(x_i)$ and $\mathcal{R}^{\pm}$ are upwind biased reconstruction operators, WENO5 reconstructions in our case. We refer the reader to [13, 14] for further details about the WENO method.

In this work we define the functions $f^{\pm,k}$ given by the Lax-Friedrichs (LF) flux-splitting $f^{\pm,k}(\Phi) = \frac{1}{2}(f(\Phi) \pm \alpha_k \Phi)$ with α_k verifying:

$$\max\{|\lambda_k(f'(\Phi))| \ / \ k = 1, \ldots, M, \ \Phi \in \mathcal{K}\} \leq \alpha_k,$$

where $\mathcal{K}$ is some relevant range where this maximal k-characteristic velocity is estimated. In many applications, specially when all characteristic fields are either genuinely nonlinear or linearly degenerate, it is enough to consider $\mathcal{K} = \{\Phi_i, \Phi_{i+1}\}$.

The characteristic fields of the MLB model are not genuinely nonlinear nor linearly degenerate, so a more sophisticated bound α_k, based on the interlacing property (2), was proposed in [6]:

$$\alpha_k = \max\{|v_i(\Phi)|, |v_{i+1}(\Phi)| \ / \ \Phi \in [\Phi_i, \Phi_{i+1}]\},$$

where $[\Phi_i, \Phi_{i+1}]$ denotes the line segment determined by $\Phi_i, \Phi_{i+1} \in \mathbb{R}^M$. The resulting scheme will be referred to as SPECINT.

Characteristic-wise schemes have a main disadvantage: the high computational cost needed to obtain the spectral decomposition of the Jacobian matrix of some problems for which no closed formulas are available. To undertake this shortcoming, a component-wise approach for these schemes was developed in [24]. For these schemes, the value of the numerical flux vector $\widehat{f}_{i+\frac{1}{2}}$ is computed by setting $l^k_l = r^k_l = \delta_{k,l}$ in (5) and $f^{\pm,k} = f^{\pm}$, for any $k, l = 1, \ldots, M$. Then, the numerical flux for the component-wise scheme reads as:

$$\widehat{f}_{i+\frac{1}{2},k} = \mathcal{R}^+ \left(f^+_{i-2,k}, \ldots, f^+_{i+2,k}; x_{i+\frac{1}{2}}\right) + \mathcal{R}^- \left(f^-_{i-1,k}, \ldots, f^-_{i+3,k}; x_{i+\frac{1}{2}}\right). \tag{6}$$

It is known that component-wise schemes obtained from global Lax-Friedrichs flux splittings $f^{\pm}$ have an oscillatory behavior, see e.g. [10], and that their numerical solutions tend to be quite diffusive, due to the global prescription of

numerical viscosity, as it could be seen for example in [6, 10]. In this work, we use a local LF flux-splitting which alleviates the excessive diffusion and the oscillatory behavior showed by its global counterpart (see [18] for more details).

4. The hybrid algorithm

Once we have given the details of the constitutive elements of our algorithm, we describe next the smoothness analysis and the corresponding computation of the numerical fluxes $\widehat{f}_{i+\frac{1}{2}}$.

To determine the local smoothness of the solution on a uniform grid on $[0, L]$ we use the procedure defined by Chiavassa and Donat in [7], adapting it to our problem. In their work, the authors presented a method based on point-value multiresolution transform used to detect regions with singularities.

From the discrete computational data $\phi_{j,i} = \phi_j(x_i, t)$, for each component $j = 1, \ldots, M$ and spatial location $i = 1, \ldots, N$, we can compute a set of interpolated values of $\phi_{j,i}$, denoted by $\overline{\phi}_{j,i}$, considering a 4-point centered interpolatory technique as:

$$\overline{\phi}_{j,i} = \mathcal{I}[x_i; \phi_j] = \frac{9}{16}(\phi_{j,i+1} + \phi_{j,i-1}) - \frac{1}{16}(\phi_{j,i+3} + \phi_{j,i-3}). \tag{7}$$

The values $\phi_{j,i}$ are extended when $i \notin \{1, \ldots, N\}$ as follows:

$$\phi_{j,i} = \begin{cases} \phi_{j,1-i} & i < 1 \\ \phi_{j,2M+1-i} & i > N. \end{cases} \tag{8}$$

Using this set of interpolated values, we can define the coefficients $\gamma_{j,i}$ as the absolute value of the difference between exact and interpolated data:

$$\gamma_{j,i} = \left| \phi_{j,i} - \overline{\phi}_{j,i} \right|.$$

Note that the coefficients $\gamma_{j,i}$ are interpolation errors which can be used directly as "sensors" in order to localize non-smooth behavior.

Once this set of coefficients is computed, we use them to create a boolean flag vector for each component, whose values (0 or 1) determine the choice of the procedure to evaluate $\widehat{f}_{i+\frac{1}{2}}$. For each component and for each spatial location, we define the flag vector $b_j = (b_{j,i})_{i=1,\ldots,N}$ as:

$$b_{j,i} = \begin{cases} 1, & \text{if } \max\limits_{k=-1,0,1} \gamma_{j,i+k} \geq \varepsilon \max\limits_{i} \gamma_{j,i}; \\ 0, & \text{if } \max\limits_{k=-1,0,1} \gamma_{j,i+k} < \varepsilon \max\limits_{i} \gamma_{j,i}, \end{cases}$$

where ε is a given tolerance parameter, $0 < \varepsilon < 1$, which controls the difference between the numerical values and the interpolated values. Notice that by considering $max_{k=-1,0,1}\gamma_{j,i+k}$ we add a safety region of one cell surrounding the cells that would have been flagged by only regarding the local detail $\gamma_{j,i}$.

Finally, using all the boolean flag vectors computed for each component, we can define the boolean flag vector $B_i = \vee_{j=1}^{M} b_{j,i}$.

The behavior of the solution of the problems we are focused on at the boundaries is well known: near the bottom boundary non-smooth structure is created while at the top boundary the solution rapidly attains zero concentration. The extrapolation defined for the computation of the interpolated values near the boundaries (8) would be exact near the top boundary, due to the constancy of the solution. At the bottom boundary the interpolated values $\overline{\phi}_{j,i}$ would not be accurate approximations of the real values $\phi_{j,i}$ assuring this region to be flagged over time. Therefore, it is not necessary to use a higher-order extrapolation near the boundaries.

Notice that this thresholding algorithm takes into consideration that large values of the coefficients $\gamma_{j,i}$ correspond to non-smooth regions of the solution and produces a flagged region containing the singularities that are present in all the components of the solution.

Finally, for each $i = 1, \ldots, N$, we compute the numerical flux $\widehat{f}_{i+\frac{1}{2}}$ depending on the value of the boolean flags B_j as:

- If $B_i = 1$ or $B_{i+1} = 1$, the location has been flagged as non-smooth and a precise computation of the numerical flux is required, so we compute $\widehat{f}_{i+\frac{1}{2}}$ with the characteristic based version (5).
- Otherwise we are located in a smooth region, so we compute $\widehat{f}_{i+\frac{1}{2}}$ with the component-wise version (6).

As Chiavassa and Donat stated in their work [7], when using a Runge-Kutta ODE solver it is not necessary to compute the flag vector in each Runge-Kutta stage in (4). As $\Phi^{(1)}$ is an approximation of Φ^{n+1}, it contains similar non-smooth structures at the same places, thus the flag coefficients obtained from the computation of $\Phi^{(1)}$ can be used to compute $\Phi^{(2)}$ from $\Phi^{(1)}$ and Φ^{n+1} from $\Phi^{(2)}$, thus avoiding the computation of the flag coefficients in two of the three stages of the Runge-Kutta ODE solver. With this modification, we can reduce the computational cost of the hybrid scheme, without losing accuracy in the numerical results.

The CPU gain of this algorithm stems from the fact that the cost of the component-wise approximation of the scheme is significantly smaller than the characteristic based approach cost. For example, for the polydisperse sedimentation tests that we will see in the next section, the cost of the component-wise approximation of the scheme is about 4.5 and 18 times smaller, respectively, than the characteristic-based approach cost, as it could be seen in [18]. The efficiency of the scheme depends on the problem.

5. Numerical experiments

In this section we present and analyze the results obtained with our hybrid algorithm applied to two typical sedimentation experiments for batch settling

in a column that one can find in the literature. The value of the threshold parameter ε that we are going to use in all the subsequent tests is $\varepsilon = 0.1$.

We use a varying time step Δt computed as:

$$\Delta t = \frac{0.5\Delta x}{C},$$

where C is an estimate of the maximal characteristic velocity of the approximated solution at the given time step. The computation of this parameter depends on the scheme used. For the SPECINT scheme, the estimate is based on the computed eigenvalues. For the component-wise scheme, we use the bounds on the eigenvalues quoted in (2). For our hybrid scheme we just merge both strategies, using the computed eigenvalues, determined in trouble regions, and the approximated eigenvalues, computed using the interlacing property (2) in smooth regions, to compute the parameter C.

The edges of the spatial domain $[0, L]$ are the cell interfaces $x_{\frac{1}{2}} = 0$ and $x_{N+\frac{1}{2}} = L$. In order to ensure the conservation of each species throughout the time evolution, our implementation for the zero-flux boundary conditions is as follows:

$$\hat{f}_{\frac{1}{2}} = \hat{f}_{N+\frac{1}{2}} = 0.$$

The L^1-error for an approximation $(\phi_{j,i})$, $i = 1, \ldots, N$, $j = 1, \ldots, M$ to the solution at the cell centers x_i and given time t, $(\phi_j(x_i, t))$, is computed as

$$\frac{1}{N} \sum_{i=1}^{N} \sum_{j=1}^{M} |\phi_{j,i}^{\text{ref}} - \phi_{j,i}|$$

where $(\phi_{j,i}^{\text{ref}})$ is a reference solution computed at a fairly high resolution, with SPECINT scheme in our case, and interpolated at the coarse cell centers.

In the following experiments we work with normalized depth, consequently, the spatial coordinate x varies between $x = 0$ (surface of the suspension) and $x = 1$ (bottom of the settling column).

Test 1.

We consider the standard test case, proposed by Greenspan and Ungarish in [11], defined by an initially homogeneous suspension in a column of height $L =$ 0.3 m with four different species of particles with same density $\varrho_s = 2790 kg/m^3$ and different normalized sizes $d_1 = 1$, $d_2 = D_2/D_1 = 0.8$, $d_3 = D_3/D_1 = 0.6$ and $d_4 = D_4/D_1 = 0.4$ with $D_1 = 4.96 \cdot 10^{-4}$ m. The initial concentrations of the particles are $\phi_i^0 = 0.05$ for all $i = 1, \ldots, 4$, the Richardson-Zaki exponent is $n_{\text{RZ}} = 4.7$ and the maximum total concentration is $\phi_{max} = 0.68$. The density and viscosity of the fluid are $\varrho_f = 1208 kg/m^3$ and $\mu_f = 0.02416 kg/(s \cdot m)$, respectively. This test was solved numerically, e.g., in [5, 6].

In Figure 1, we display the reference solutions $\phi_1, \ldots, \phi_4$ and the global density $\phi = \sum_i \phi_i$, computed with the SPECINT scheme with $N = 6400$ cells and $t = 300$s. In Fig. 2 we display some enlarged views of the numerical approximations of ϕ_4 computed with a local Lax-Friedrichs component-wise scheme

(LLF), our hybrid scheme (HYB-LLF) and the characteristic-based SPECINT scheme, using two meshes of $N = 400$ and $N = 1600$ cells.

It can be seen throughout those pictures that the approximations obtained with the hybrid scheme are less oscillatory than their LLF counterparts, being quite similar to the SPECINT approximations. The conclusions about the qualitative behavior of the approximations that we could draw from inspection of the other components would be similar to those obtained for our choice.

In Figure 3 we show the numerical solutions and the flag vectors obtained using meshes of $N = 100$, 400 and 1600 cells. As we expect, when we use coarser meshes the flagged area is wider and could include some smooth regions, specially small smooth regions located between shocks. But when we refine the mesh, the flagged regions fit exactly with regions with sharp transitions and strong shocks. In Figure 4 we can see how the numerical solutions and the flag vectors evolve with time for a fine mesh of $N = 1600$ cells.

To perform quantitative assessments, in Table 1 and Figure 5 we show the approximate L^1-errors and the CPU times for this test. We have run each of the schemes for $N = 100$, 200, 400, 800 and 1600 and recorded its CPU time for the execution and approximate L^1-error. Each symbol in a given graphic corresponds to a number N of cells.

As could be expected from the previous comments, our hybrid scheme is more accurate than the LLF scheme, the SPECINT being of course the most accurate. But when we take into account computational times, our hybrid scheme takes about 2.5 times less computational time to achieve a given error level and is consequently more efficient than SPECINT scheme, as can be deduced from Fig. 5.

The accuracy of the results depends on the value of the parameter ε. The wider the flagged regions are the more accurate the approximations obtained are. The parameter ε has to be tuned having in mind that we seek an equilibrium between accuracy and computational time to obtain not only accurate results but efficient methods. In these experiments by choosing a smaller value of the parameter ε, $\varepsilon < 0.1$, the results in terms of accuracy do not improve significantly but the computational times increase due to the use of wide flagged regions.

As shown in Table 3, when the parameter ε increases, the number of fluxes computed with the SPECINT scheme diminishes. As a consequence, the CPU time diminishes too, but the errors increase, getting closer to the errors given by LLF scheme as shown in Table 2.

We compare the results obtained with our hybrid scheme with those obtained when using an adaptive multiresolution framework based on the work developed in [4, 12]. This multilevel algorithm consists in substituting the direct computation of the numerical divergences $\Delta x^{-1}(\widehat{f}_{i+\frac{1}{2}} - \widehat{f}_{i-\frac{1}{2}})$ on the finest grid by a multilevel strategy that saves computational time by interpolating from coarse levels at regions not tagged by the same procedure that we have used in our hybrid scheme to determine the boolean flag vector, see [8] for more information about the multilevel strategy. We use grids of 800, 1600 and 3200

nodes with 4, 5 and 6 levels of multiresolution respectively, in order to have a coarser mesh with $N_0 = 100$ nodes in all cases. We use two different values for the tolerance parameter *tol*, which plays the same role as the parameter ε in the hybrid scheme.

As it can be seen in Table 4, the hybrid scheme requires quite less computational effort than the multiresolution scheme to achieve a similar numerical accuracy.

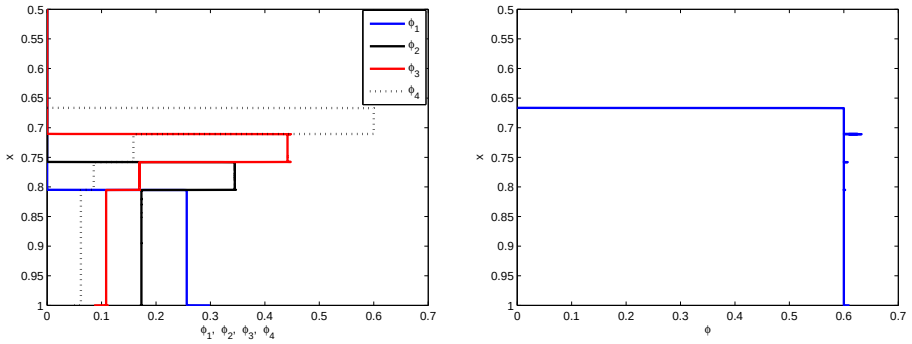

(a) (b)

Figure 1: Reference solutions of test 1. (a) $\phi_1, \ldots, \phi_4$ and (b) $\phi = \sum_i \phi_i$ computed with SPECINT scheme for $t = 300$s and N=6400 cells.

N	LLF		HYB-LLF		SPECINT	
	CPU	error	CPU	error	CPU	error
100	0.715	24.88	1.883	6.836	3.146	6.753
200	2.479	13.49	5.609	3.784	10.53	3.782
400	9.366	6.823	17.41	1.718	49.02	1.676
800	35.43	3.372	62.22	0.851	153.3	0.850
1600	145.3	1.596	240.1	0.366	665.3	0.369

Table 1: Approximate L^1-errors ($\times 10^{-3}$) and CPU times (seconds) for test 1 with parameter $\varepsilon = 0.1$ and $t = 300$s.

We describe now a reasonable strategy for the selection of the parameter ε. Given some details $\gamma_{j,i}$, one can define the function $\beta_j(r) = \beta_j[\gamma](r)$

$$\beta_j(r) = \frac{\sum_i \{\gamma_{j,i}/\gamma_{j,i} > r\}}{\sum_i \gamma_{j,i}}. \tag{9}$$

The value $\beta_j(r) \in [0,1]$ is the ratio between the sum of the details $\gamma_{j,i}$ that are above the threshold r with respect to the sum of all the details. With these functions and a number $p \in (0,1)$ we can compute

$$\varepsilon = \varepsilon(p) = \max\{r_* > 0 / \min_j \beta_j(r_*) > p\}. \tag{10}$$

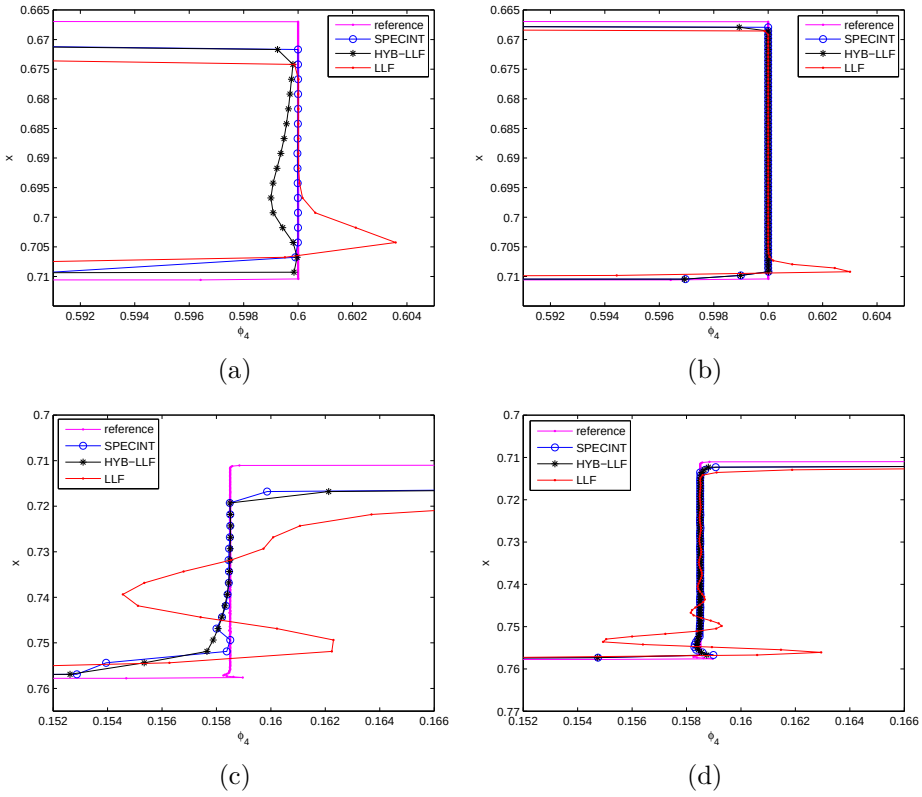

Figure 2: Enlarged views of some discontinuities present in the numerical approximation of ϕ_4 for test 1 computed with $t = 300$s and $N = 400$ ((a) and (c)) and $N = 1600$ ((b) and(d)).

N	$\varepsilon = 0.75$		$\varepsilon = 0.5$		$\varepsilon = 0.25$	
	CPU	error	CPU	error	CPU	error
100	1.423	10.18	1.684	8.221	1.642	6.800
200	4.831	6.116	5.012	4.453	5.231	3.771
400	16.01	3.106	16.23	2.715	16.99	1.739
800	57.95	1.072	58.41	0.874	60.07	0.852
1600	227.8	0.699	216.1	0.574	218.2	0.556
N	$\varepsilon = 0.1$		$\varepsilon = 0.05$		$\varepsilon = 0.01$	
	CPU	error	CPU	error	CPU	error
100	1.883	6.836	2.011	6.849	2.455	6.853
200	5.609	3.784	6.010	3.781	6.974	3.782
400	17.41	1.718	17.64	1.721	18.82	1.687
800	62.22	0.851	63.84	0.848	65.02	0.845
1600	240.1	0.366	245.0	0.365	248.3	0.366

Table 2: Approximate L^1-errors ($\times 10^{-3}$) and CPU times (seconds) for test 1 obtained by the hybrid scheme with different values of the parameter ε and $t = 300$s.

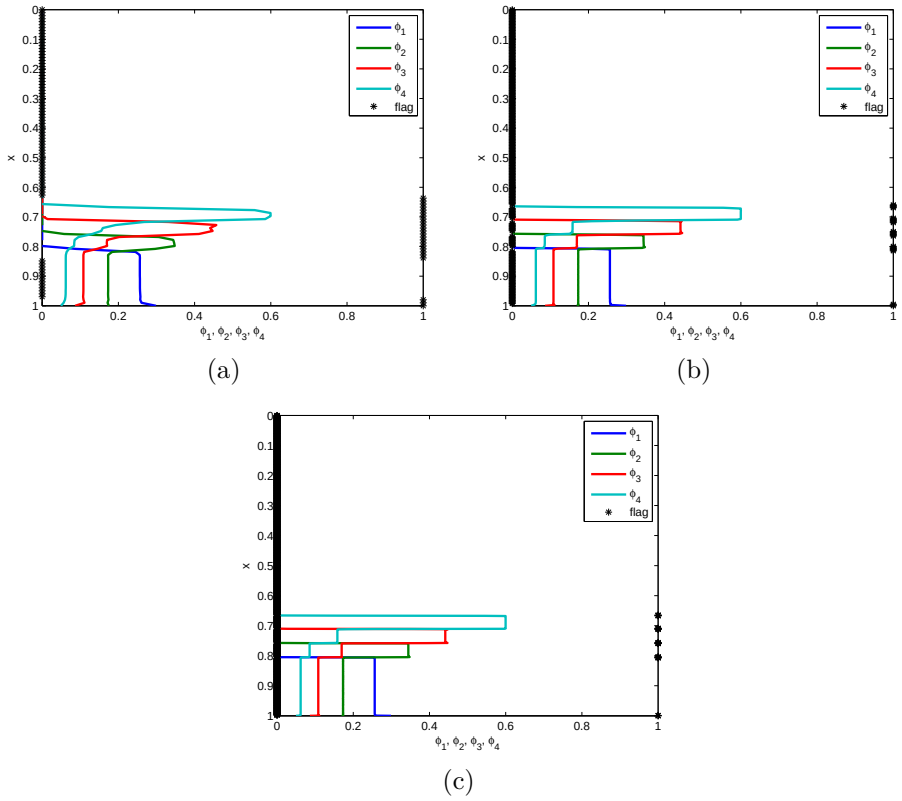

Figure 3: Numerical solutions and flag vectors for test 1 with $t = 300$s and (a) $N = 100$ and (b) $N = 400$ and (c) $N = 1600$ cells.

N	$\varepsilon = 0.01$	$\varepsilon = 0.05$	$\varepsilon = 0.1$	$\varepsilon = 0.25$	$\varepsilon = 0.5$	$\varepsilon = 0.75$
100	36.9 %	30.5 %	26.2 %	21.3 %	13.4 %	9.91 %
200	23.6 %	19.7 %	16.9 %	9.84 %	6.72 %	5.06 %
400	12.7 %	10.2 %	8.26 %	5.57 %	2.91 %	2.43 %
800	6.74 %	5.22 %	4.89 %	3.24 %	2.32 %	1.19 %
1600	3.03 %	2.71 %	2.01 %	1.33 %	0.81 %	0.58 %

Table 3: Percentage of numerical fluxes computed with SPECINT scheme in test 1 depending on the value of the parameter ε with $t = 300$s.

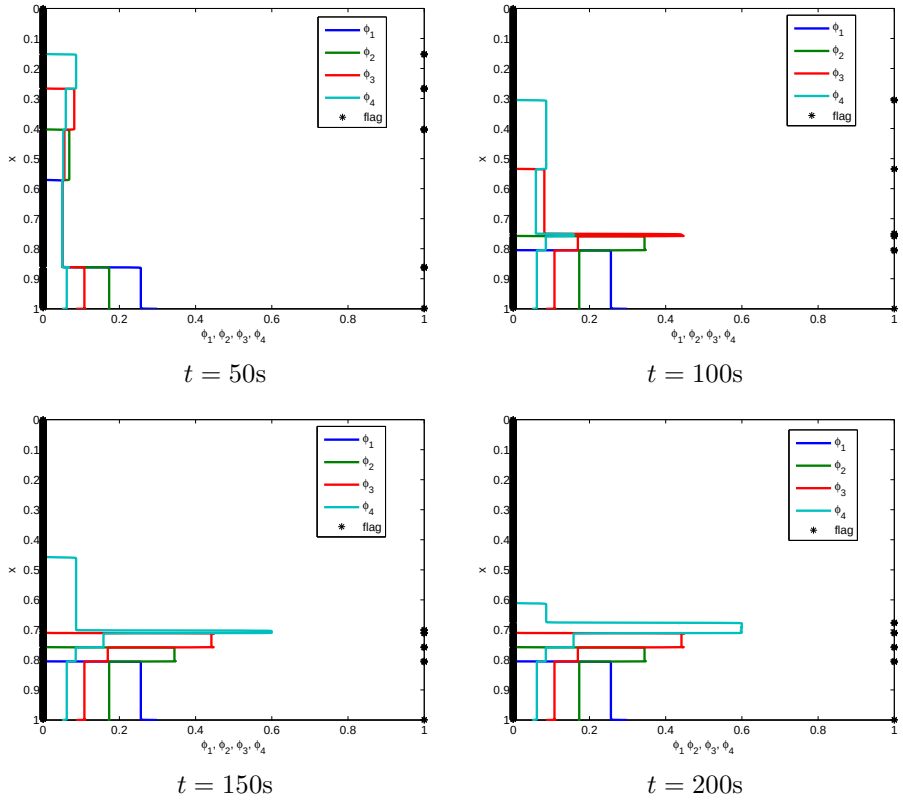

Figure 4: Time evolution of the numerical solutions and flag vectors of test 1 computed with $t = 300$s and $N = 1600$ cells.

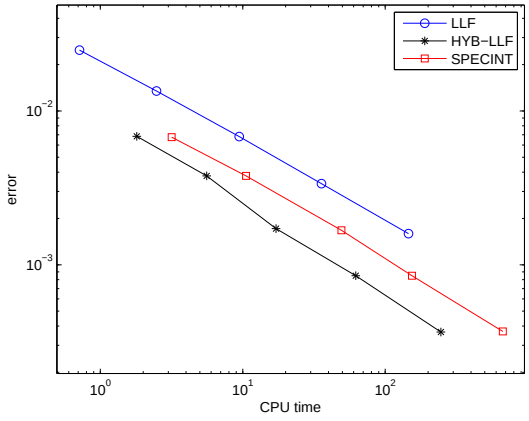

Figure 5: CPU time - error comparison for test 1 using $t = 300$s.

N	HYB-LLF $\varepsilon = 0.1$		MR $tol = 10^{-2}$		MR $tol = 10^{-3}$		SPECINT	
	CPU	error	CPU	error	CPU	error	CPU	error
800	62.22	8.51	98.19	12.0	116.1	8.89	154.0	8.50
1600	240.1	3.66	223.3	5.16	265.3	4.03	669.6	3.69
3200	1287.7	1.43	628.3	3.64	867.7	2.16	4784.7	1.45

Table 4: Approximate L^1-errors ($\times 10^{-4}$) and CPU times (seconds) for test 1 obtained by the hybrid scheme and the scheme with a multiresolution framework with different values of the parameter tol with $t = 300$s.

That is, ε is the maximal r_* such that all the graphs of β_j, $j = 1, \ldots, M$ for $r \in [0, r_*]$ lies above p.

In Figure 6 we display the graph of β_j, $j = 1, 2, 3, 4$, based on the details obtained for $N = 200$ and $t = 300s$. We deduce that selecting ε between 0.074 and 0.14 would yield that the most important details would be flagged. Figure 7 shows the graph of β_1 for $N = 100, 200, 400, 800, 1600$ and $t = 300s$ and Figure 8 shows the graph of β_1 for $N = 1600$ and $t = 50, 100, 150, 200$. These pictures suggest that setting $p \in [0.8, 0.9]$ yields a reasonable parameter $\varepsilon = \varepsilon(p)$, in terms of efficiency, in quite a robust manner with respect to resolution and simulated time.

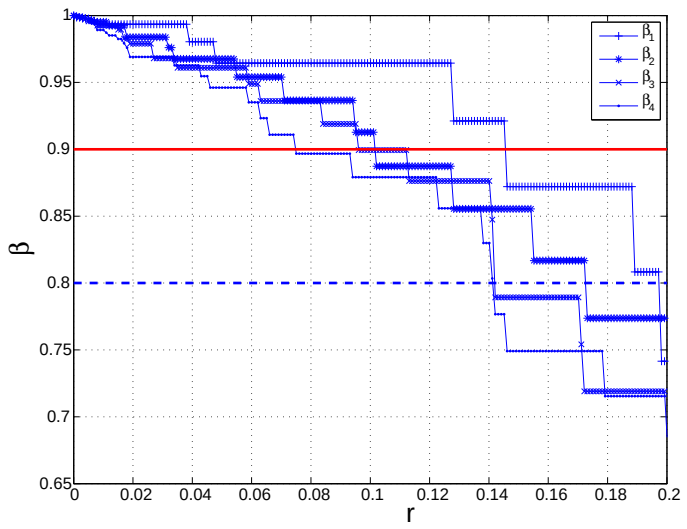

Figure 6: Graph of β_j function, $j = 1, 2, 3, 4$ for details computed with $N = 200$ and $t = 300s$.

Test 2.

The next experiment consists on the batch settling of an initially homogeneous suspension with eleven different species in a column of height $L = 0.935$ m, with initial concentrations ϕ_i^0, diameters D_i and normalized diameters $d_i =$

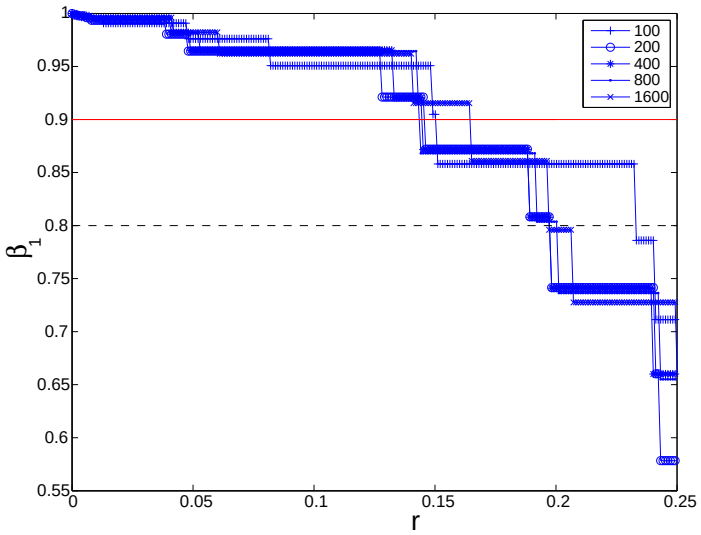

Figure 7: Graph of β_1 function for details computed with $N = 100, 200, 400, 800, 1600$ and $t = 300s$.

D_i/D_1 of the particles given in Table 5. This test is based on experimental data from [21].

We consider the Richardson-Zaki exponent $n_{RZ} = 4.65$ and maximum total concentration $\phi_{max} = 0.641$. The other parameters are those of the previous test.

In Figure 9 we show the reference solutions for $\phi_1, \ldots, \phi_{11}$ and $\phi = \sum_i \phi_i$, computed with the SPECINT scheme with $N = 6400$ cells and $t = 300$s.

The appearance of very thin layers of sediment of the smaller particles at the top of the sedimentation vessel poses severe difficulties for the numerical schemes to capture them. Therefore, to obtain accurate results we need to use an efficient shock capturing scheme and a very fine mesh as illustrates Figure 10 where we can see that when using a coarser mesh of $N = 400$ cells the results are very imprecise with all the schemes, while when we use a finer mesh with $N = 1600$ the quality of the results improve but they are far away from the results obtained using a grid with $N = 6400$ cells.

In this specific experiment the main drawback of the characteristic-wise scheme is the high computational cost needed to obtain the spectral decomposition of the Jacobian matrix. We need to compute at least one eigenvalue and one eigenvector for each component and for each spatial location. Since we deal with eleven components and that a very fine mesh is mandatory, the simulation requires a huge CPU time.

In Table 6 we display the computational times and the L^1-errors obtained by the component-wise LLF scheme, our hybrid scheme and the characteristic-wise SPECINT scheme ran with very fine meshes of $N = 1600$, 3200 and 6400

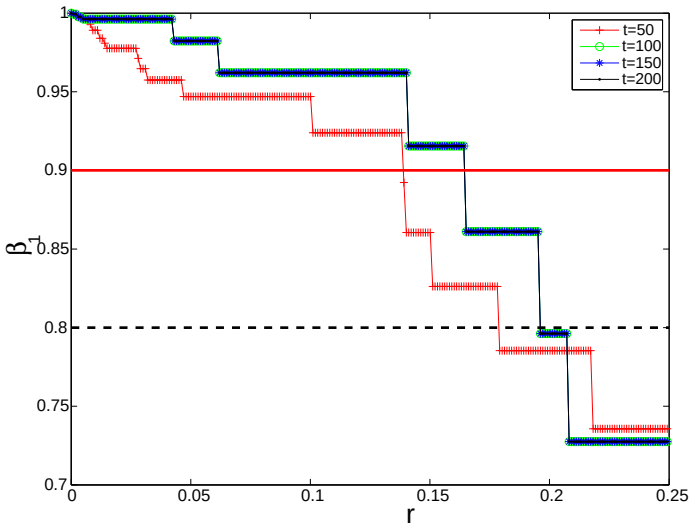

Figure 8: Graph of β_1 function for details computed with $N = 1600$ and $t = 50, 100, 150, 200s$. The graphs for $t = 100, 150, 200$ are coincident.

cells. As we expect, the SPECINT scheme is highly time consuming while our hybrid scheme takes about 10 times less computational time to achieve the same error level. Therefore, the proposed hybrid scheme represents a real alternative when dealing with costly solvers applied to large problems on fine grids.

We observe in Table 7 that the hybrid scheme performs better than the scheme with the multiresolution framework. When we use the multiresolution technique with a tolerance parameter $tol = 10^{-3}$ the errors obtained are slightly smaller than the errors for the hybrid scheme but when considering CPU times, the hybrid scheme takes approximately 3.5 times less computational time to compute the numerical solutions. Thus, in this case, the hybrid scheme is more efficient than the scheme with the multiresolution technique.

i	1	2	3	4	5	6
$\phi_i^0[10^{-3}]$	0.435	3.747	14.420	32.603	47.912	47.762
$D_i[10^{-5}]$	8.769	8.345	7.921	7.497	7.073	6.649
d_i	1.000	0.952	0.903	0.855	0.807	0.758
i	7	8	9	10	11	
$\phi_i^0[10^{-3}]$	32.663	15.104	4.511	0.783	0.060	
$D_i[10^{-5}]$	6.225	5.801	5.377	4.953	4.529	
d_i	0.710	0.662	0.613	0.565	0.516	

Table 5: Initial concentrations ϕ_i^0, real and normalized diameters D_i and d_i of test 2.

In Figure 11 we display the graph of $\min_{j=1,\ldots,11} \beta_j$, based on the details

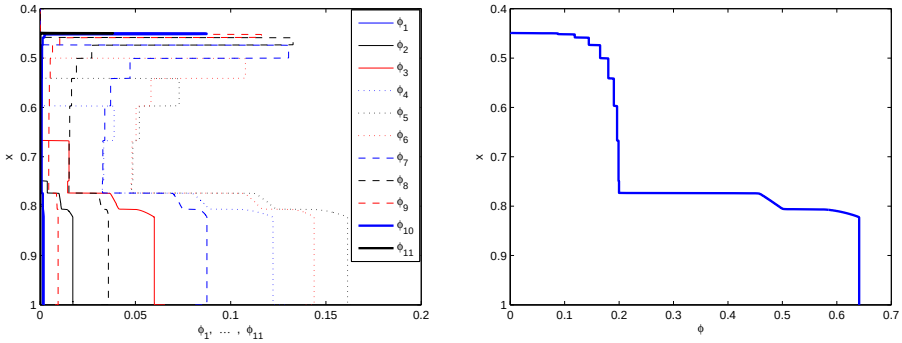

(a) (b)

Figure 9: Reference solutions of test 2. (a) $\phi_1, \ldots, \phi_{11}$ and (b) $\phi = \sum_i \phi_i$ computed by SPECINT scheme with $N = 6400$ cells and $t = 300$s.

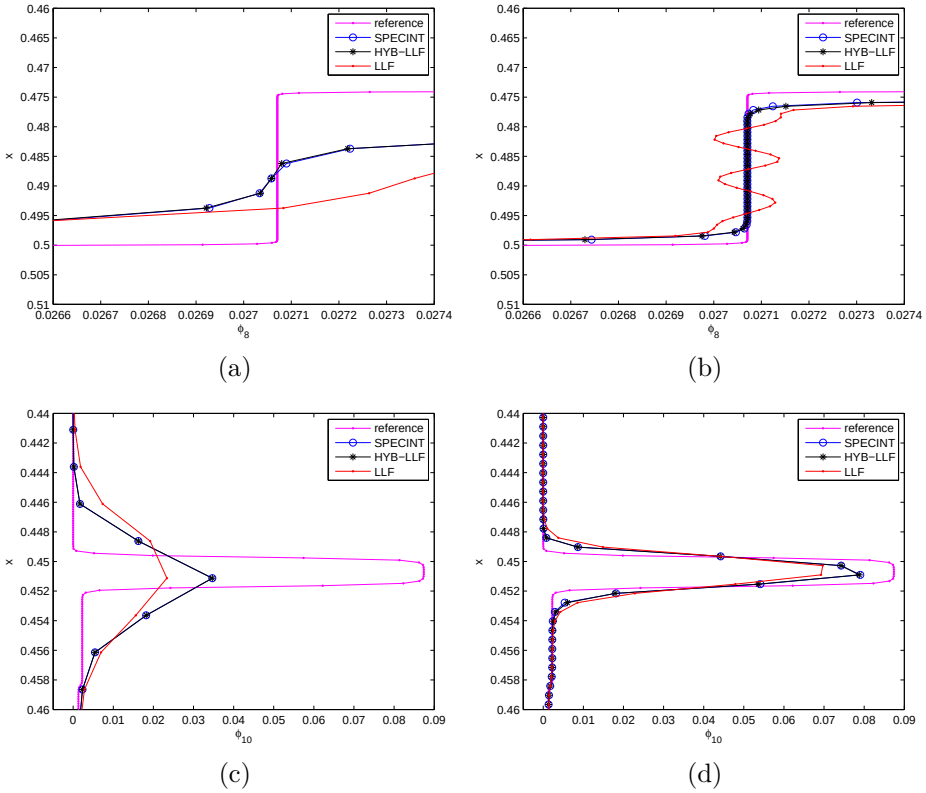

(a) (b)

(c) (d)

Figure 10: Enlarged views of discontinuous regions of ϕ_8, ((a) and (b)), and ϕ_{10}, ((c) and (d)), for test 2 computed with $t = 300$s and $N = 400$ *(left)* and $N = 1600$ *(right)*.

N	LLF		HYB-LLF		SPECINT	
	CPU	error	CPU	error	CPU	error
1600	84.82	0.834	177.5	0.621	1507.5	0.594
3200	468.8	0.360	589.8	0.244	5920.2	0.227
6400	1789.0		2140.2		23713.1	

Table 6: Approximate L^1-errors ($\times 10^{-3}$) and CPU times (seconds) for test 2 with $t = 300$s.

N	HYB-LLF $\varepsilon = 0.1$		MR $tol = 10^{-2}$		MR $tol = 10^{-3}$		SPECINT	
	CPU	error	CPU	error	CPU	error	CPU	error
800	59.34	13.8	167.2	13.9	175.6	13.6	401.3	13.6
1600	177.5	6.22	425.8	6.22	499.5	5.95	1507.5	5.94
3200	589.8	2.45	1508.2	2.86	2464.2	2.31	5920.2	2.27

Table 7: Approximate L^1-errors ($\times 10^{-4}$) and CPU times (seconds) for test 2 obtained by the hybrid scheme and the scheme with a multiresolution framework different values of the parameter *tol* and $t = 300$s.

obtained for $N = 1600$ and $t = 300s$. We deduce that selecting ε between 0.04 and 0.09 would yield that the most important details would be flagged.

6. Conclusions

We have presented a cost-effective alternative to characteristic based HRSC finite difference WENO schemes for polydisperse sedimentation problems. Merging the characteristic based scheme with a component-wise approach for this scheme, we have developed a hybrid scheme that uses characteristic information only on a neighborhood of a discontinuity, where more accuracy is needed to compute precise numerical solutions.

The numerical results showed in this paper point out that, although there are no memory savings, there is a significant reduction of the computational time when using the hybrid scheme proposed, which offers the possibility of obtaining a high-resolution numerical solution on a very fine grid with a reasonable cost.

Acknowledgments

We want to express our gratitude to the reviewers, whose comments have helped to improve this work. The authors acknowledge financial support from MINECO projects MTM2011-22741 and MTM2014-54388. M.C. Martí is supported by Proyecto FONDECYT de Postdoctorado 2015, N. 3150140.

References

[1] M. J. Berger and P. Colella, *Local adaptive mesh refinement for shock hydrodynamics*, J. Comput. Phys., 82 (1989), pp. 64–84.

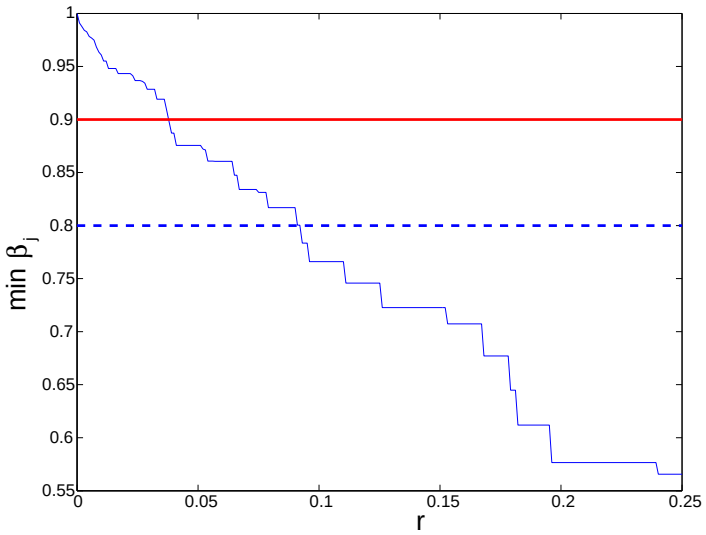

Figure 11: Graph of $\min_{j=1,\ldots,11} \beta_j$ function for details computed with $N = 1600$ and $t = 300s$.

[2] M. J. Berger and J. Oliger, *Adaptive mesh refinement for hyperbolic partial differential equations*, J. Comput. Phys., 53 (1984), pp. 484–512.

[3] S. Berres, R. Bürger, K. H. Karlsen, and E. M. Tory, *Strongly degenerate parabolic-hyperbolic systems modeling polydisperse sedimentation with compression*, SIAM J. Appl. Math., 64 (2003), pp. 41–80.

[4] B. L. Bihari and A. Harten, *Multiresolution schemes for the numerical solution of 2-D conservation laws*, I. SIAM J. Sci. Comput., 18(2) (1997), pp. 315–354.

[5] R. Bürger, F. Concha, K.-K. Fjelde, and K. H. Karlsen, *Numerical simulation of the settling of polydisperse suspensions of spheres*, Powder Technol., 113 (2000), pp. 30–54.

[6] R. Bürger, R. Donat, P. Mulet, and C. A. Vega, *On the implementation of WENO schemes for a class of polydisperse sedimentation models*, J. Comput. Phys., 230 (2011), pp. 2322–2344.

[7] G. Chiavassa and R. Donat, *Point-value multiscale algorithms for 2D compressible flows*, SIAM J. Sci. Comput., 20 (2001), pp. 805–823.

[8] G. Chiavassa, R. Donat and A. Martinez-Gavara, *Cost-effective multiresolution schemes for shock computations*, ESAIM: PROCEEDINGS, 29 (2009), pp. 8–27.

[9] B. Costa and W. S. Don, *Multi-domain hybrid spectral-WENO methods for hyperbolic conservation laws*, J. Comput. Phys., 224(2) (2007), pp. 970-991.

[10] R. Donat and P. Mulet, *A secular equation for the Jacobian matrix of certain multispecies kinematic flow models*, Numer. Methods Partial Differential Equations, 26 (2010), pp. 159–175.

[11] H. Greenspan and M. Ungarish, *On hindered settling of particles of different sizes*, Int. J. Multiphase Flow, 8 (1982), pp. 587–604.

[12] A. Harten, *Multiresolution algorithms for the numerical solution of hyperbolic conservation laws*, Comm. Pure Appl. Math., 48 (1995), pp. 1305–1342.

[13] G.-S. Jiang and C.-W. Shu, *Efficient implementation of weighted eno schemes*, J. Comput. Phys., 126 (1996), pp. 202–228.

[14] X.-D. Liu, S.Osher, and T. Chan, *Weighted essentially non-oscillatory schemes*, J. Comput. Phys., 115 (1994), pp. 200–212.

[15] G. Liu and J. Qiu, *Hybrid weighted essentially non-oscillatory schemes with different indicators*, J. Comput. Phys., 229 (2010), pp. 8105-8129.

[16] M. J. Lockett and K. S. Bassoon, *Sedimentation of binary particle mixtures*, Powder Technol., 24 (1979), pp. 1–7.

[17] J. H. Masliyah, *Hindered settling in a multiple-species particle system*, Chem. Eng. Sci., 34 (1979), pp. 1166–1168.

[18] M. C. Martí and P. Mulet, *Some techniques for improving the resolution of finite difference component-wise WENO schemes for polydisperse sedimentation models*, App. Num. Math., 78 (2014), pp. 1–13.

[19] Y-X. Ren, M. Liu and H. Zhang, *A characteristic-wise hybrid compact-WENO scheme for solving hyperbolic conservation laws*, J. Comput. Phys., 192 (2003), pp. 365-386.

[20] J. Richardson and W. Zaki, *The sedimentation of a suspension of uniform spheres under conditions of viscous flow*, Chemical Engineering Science, 3 (1954), pp. 65–73.

[21] P. T. Shannon, E. Stroupe, and E. M. Tory, *Batch, continuous thickening*, Ind. Eng. Chem. Fund., 2 (1963), pp. 203–211.

[22] C.-W. Shu and S. Osher, *Efficient implementation of essentially non-oscillatory shock-capturing schemes*, J. Comput. Phys., 77 (1988), pp. 439–471.

[23] ———, *Efficient implementation of essentially non-oscillatory shock-capturing schemes, ii*, J. Comput. Phys., 83 (1989), pp. 32–78.

[24] M. Zhang, C.-W. Shu, G. Wong, and S. Wong, *A weighted essentially non-oscillatoy numerical scheme for a multi-class lighthill-whitham-richards traffic flow model*, J. Comput. Phys., 191 (2003), pp. 639–659.